



**HAL**  
open science

## Propagating uplift controls on high-elevation, low-relief landscape formation in the southeast Tibetan Plateau

X.P. Yuan, K.L. Huppert, J. Braun, X. Shen, J. Liu-Zeng, Laure Guerit, S.G. Wolf, J.F. Zhang, Marc Jolivet

### ► To cite this version:

X.P. Yuan, K.L. Huppert, J. Braun, X. Shen, J. Liu-Zeng, et al.. Propagating uplift controls on high-elevation, low-relief landscape formation in the southeast Tibetan Plateau. *Geology*, 2022, 50 (1), pp.60-65. 10.1130/G49022.1 . insu-03350035

**HAL Id: insu-03350035**

**<https://insu.hal.science/insu-03350035>**

Submitted on 22 Sep 2021

**HAL** is a multi-disciplinary open access archive for the deposit and dissemination of scientific research documents, whether they are published or not. The documents may come from teaching and research institutions in France or abroad, or from public or private research centers.

L'archive ouverte pluridisciplinaire **HAL**, est destinée au dépôt et à la diffusion de documents scientifiques de niveau recherche, publiés ou non, émanant des établissements d'enseignement et de recherche français ou étrangers, des laboratoires publics ou privés.



26 incision of the large mainstem rivers. The propagating uplift also produces spatial and temporal  
27 exhumation patterns and river profile morphologies that match observations. Our modeling  
28 therefore reconciles geomorphic observations with geodynamic models of uplift of the SE  
29 Tibetan Plateau, and provides a simple mechanism to explain low-relief surfaces observed in  
30 several mountain belts on Earth.

31

## 32 INTRODUCTION

33 High-elevation, low-relief surfaces are ubiquitous in many mountain belts (e.g., [Epis and](#)  
34 [Chapin, 1975](#); [Kennan et al., 1997](#); [Babault et al., 2005](#); [van der Beek et al., 2009](#)). They are  
35 often interpreted to be remnant surfaces of paleo-landscapes and are thus widely used as  
36 geomorphic markers to constrain tectonic uplift and landscape evolution ([Clark et al., 2006](#)).  
37 However, the origin of high-elevation, low-relief surfaces remains highly disputed (e.g., [Clark](#)  
38 [et al., 2006](#); [Liu-Zeng et al., 2008](#); [Yang et al., 2015](#); [Whipple et al., 2017](#); [Bosch et al., 2018](#);  
39 [Fox et al., 2020](#)), with previous studies mainly proposing that they either represent a relict pre-  
40 uplift low-relief surface, uplifted and eroded by a wave of upstream incision instigated by an  
41 increase in rock uplift ([Clark et al., 2006](#); [Whipple et al., 2017](#)), or that they formed *in-situ* by  
42 tectonic shortening and consequent drainage reorganization ([Yang et al., 2015](#)). This debate  
43 exists especially in the SE Tibetan Plateau where the low-relief surfaces are widely observed  
44 (Fig. 1A).

45 Three of the world's largest rivers (Salween, Mekong and Yangtze) run from the central Tibetan  
46 Plateau across the SE plateau margin (Fig. 1B). High-elevation, low-relief surfaces at elevations  
47 4-6 km above sea level and perched 2-3 km above deep adjacent valleys occupy the headwaters  
48 and interfluves of the Three Rivers (Fig. 1B; [Clark et al., 2006](#)). Thermochronologic data  
49 suggest that rapid incision has been focused within these valleys, with accelerated incision  
50 starting at >10–20 Ma ([Clark et al., 2005](#); [Ouimet et al., 2010](#); [Tian et al., 2014](#); [Liu-Zeng et](#)

51 [al., 2018](#)). In contrast, the low-relief surfaces in the headwaters and interfluves have  
52 experienced little erosion during the Cenozoic ([Clark et al., 2006](#)), with thermochronologic ages  
53 mainly at ~50 Ma ([Li et al., 2019](#)). The long-term coexistence of deep valleys and low-relief  
54 surfaces raises fundamental questions about (i) the factors controlling the formation of  
55 extensive low-relief surfaces, and (ii) the survival of the low-relief surfaces above deep valleys.  
56 Synthesized structural analyses ([Wang et al., 2014; Li et al., 2015](#)) and thermochronologic ages  
57 ([Li et al., 2019](#)) show a younging trend from the central plateau to the SE margin, suggesting  
58 that the Tibetan Plateau may have progressively grown southeastward from the central plateau  
59 since the Eocene. This uplift pattern is consistent with various geodynamic models and geologic  
60 data, which show that many mountain belts grow first to a certain height and then expand  
61 laterally in an outward propagation sequence characterized by successive marginal uplift ([e.g.,](#)  
62 [Jammes and Huisman, 2012; Wolf et al., 2021](#)).

63 By translating this information into a simple kinematic uplift function and using a landscape  
64 evolution model of long-term fluvial erosion and sediment transport ([Yuan et al., 2019](#); Data  
65 Repository Text DR1.1), we investigate whether the propagating uplift is responsible for  
66 generating the observed low-relief surfaces.

67

## 68 **FORMATION OF BROAD HIGH-ELEVATION, LOW-RELIEF SURFACES**

69 Our models start from an initially random surface with  $\leq 100$  m of relief, run for 50 Myr, and  
70 shorten uniformly NW-SE and non-uniformly SW-NE (Text DR1.2). In addition to this  
71 horizontal deformation, the modeled landscape is subject to a propagating wave of 0.23 mm/yr  
72 vertical uplift (Text DR1.3; Fig. 2A) to simulate the outward-propagating growth of the plateau,  
73 implied by the thermochronologic and structural data ([Wang et al., 2014; Li et al., 2019](#)). Uplift  
74 rates at a given point on the landscape are initially zero, gradually increase to 0.23 mm/yr with  
75 passage of the propagating uplift wave, then gradually reduce back to zero.

76 Our simulation shows that propagating uplift promotes the progressive formation of elongated,  
77 NE-SW-spanning river basins (Fig. 2A). The initial propagating uplift forms narrow, parallel  
78 drainages on the front slope of the propagating margin, and the elongated drainage basins  
79 extend downstream during forward propagating of the uplift. The headwaters and interfluves of  
80 rivers are characterized by high-elevation, low-relief surfaces (Fig. 2A and 2C). Our results  
81 reproduce the observed co-planarity of these low-relief surfaces (Figs. 1D-F and 2D), their  
82 height 2-3-km above adjacent valleys (Fig. 2E), as well as their progressive decrease in  
83 elevation from NW to SE across the plateau margin (Whipple et al., 2017). This consistency  
84 between modeled and observed topography supports our hypothesis that propagating uplift  
85 plays a key role in generating high-elevation, low-relief surfaces on the SE Tibetan Plateau.  
86 Regardless of the specific erosion and deposition parameters used (Fig. DR5), we show that the  
87 propagating uplift controls the first-order erosional dynamic of landscape evolution.

88

## 89 **SPATIAL AND TEMPORAL EXHUMATION PATTERNS**

90 In the deep valleys of our simulated mainstem rivers (black dots V1–V4 and curves in Fig. 3A-  
91 B), exhumation proceeds initially at a slow rate, accelerates, and then decreases after the uplift  
92 wave has passed (V3, V4), consistent with the cooling and exhumation pattern recorded by low-  
93 temperature thermochronologic data (e.g., Liu-Zeng et al., 2018; Li et al., 2019). The timing of  
94 accelerated exhumation in the mainstem valleys is spatially variable and propagates  
95 downstream (Fig. 3A-B), e.g., initiating at ~34 Ma (V4), ~25 Ma (V3), ~20 Ma (V2), and ~12  
96 Ma (V1). This temporal pattern is also consistent with compiled thermochronologic ages  
97 showing a younging trend from the central plateau (32–34°N) to the SE margin (~27°N) along  
98 the mainstem rivers (Li et al., 2019).

99 Normalized channel steepness  $k_{sn}$  (Wobus et al., 2006) is widely used to investigate spatial  
100 exhumation patterns and is defined as

101 
$$k_{sn} = SA^{m/n}, \tag{1}$$

102 where  $S$  is the channel slope,  $A$  is the drainage area, and  $m/n$  is the concavity of the river  
103 profile, taken to be 0.4 (Fig. DR2). Our modeling shows that  $k_{sn}$  is low in the headwaters (Fig.  
104 2B) and increases downstream in the mainstem rivers, reaching a peak value at the plateau  
105 margin, as observed on the SE Tibetan Plateau (Fig. 1B).

106 Upstream channel reaches in our model erode slowly at long-term rate (e.g.,  $\sim 650$  m/50 Myr =  
107 0.013 mm/yr; slope of the orange curve in Fig. 3B) and short-term rate (0.01–0.015 mm/yr; Fig.  
108 2D) matching observed erosion rates inferred from low-temperature thermochronology (0.01–  
109 0.02 mm/yr; Clark et al., 2006) and millennial basin-averaged cosmogenic  $^{10}\text{Be}$  erosion rates  
110 (0.013–0.024 mm/yr; Henck et al., 2011). Dividing the predicted 2.2 km exhumation of the  
111 major river valley (V2; dashed curve in Fig. 3B) by the  $\sim 20$  Ma onset of accelerated exhumation  
112 yields an average erosion rate of 0.11 mm/yr, which is within the range of exhumation rates  
113 ( $\sim 0.1$ – $0.3$  mm/yr) from the Miocene to present (20–0 Ma) inferred from thermochronologic  
114 data (Liu-Zeng et al., 2018). In contrast, the low-relief interfluves in our model have low long-  
115 term erosion rates ( $500$  m/ $\sim 25$  Myr =  $\sim 0.02$  mm/yr; slope of the cyan curve in Fig. 3B) matching  
116 erosion rates inferred from thermochronologic ages of late Miocene remnant surfaces ( $\sim 0.02$   
117 mm/yr; Clark et al., 2005; 2006) and consistent with millennial erosion rates derived from  
118 cosmogenic nuclide exposure ages (0.015–0.022 mm/yr; Ouimet et al., 2005; Clark et al., 2006).

119 The low-relief surfaces erode approximately ten times more slowly than the mainstem valleys  
120 and persist relatively unchanged because they lack sufficient drainage area to generate the  
121 incision rates necessary to keep pace with rapid incision of the mainstem rivers (Fig. 2A-B).  
122 This discrepancy in erosion rates arises because of the unusually elongated river network  
123 geometry produced by propagating plateau uplift, with large mainstem rivers fed predominantly  
124 by small tributaries along their length. Long, parallel mainstem rivers erode rapidly in response  
125 to this uplift while their short, drainage-area starved tributaries fail to keep pace. This unique

126 river network morphology provides an explanation for the persistence of high-elevation, low-  
127 relief surfaces and the deep entrenchment of their adjacent mainstem rivers.

128

## 129 RIVER PROFILE MORPHOLOGY

130 Rivers adjust their slopes in response to changes in uplift, so their morphology records transient  
131 landscape evolution. We use plots of elevation versus an upstream integral of drainage area,  $\chi$   
132 (Perron and Royden, 2013), to quantitatively compare modeled and observed river profiles  
133 (Text DR2). The slope of channel elevation with respect to  $\chi$  is  $k_{sn}$ . The  $\chi$ -elevation plots of the  
134 Three Rivers are convex (Fig. 1C), with a higher average  $k_{sn} = 66 \text{ m}^{0.8}$  downstream ( $<3558 \pm 380$   
135 m in elevation) and a lower average  $k_{sn} = 22 \text{ m}^{0.8}$  in the upstream headwaters. This change in  
136 steepness does not correlate with spatial variations in lithology (Yang et al., 2015) or mean  
137 annual precipitation (Figs. 1D-F and DR1).

138 We model two end-member cases: propagating vs. uniform uplift. The former case is supported  
139 by previous studies (Clark et al., 2000; Schoenbohm et al., 2006), while the latter provides a  
140 null hypothesis against which to test the propagating uplift model. The propagating uplift can  
141 explain changes in steepness (Fig. 3C), and the erodibility  $K_f$  of  $1.2 \times 10^{-6} \text{ m}^{0.2}/\text{yr}$  provides the  
142 best fit between modeled and observed  $\chi$ -elevation plots (Fig. DR4). We model the latter case  
143 of a uniform increase in rock uplift to reach the same final elevation  $h_f$  (Equation DR3) from  
144 the initial elevation  $h_i$  of random  $\leq 100$ -m white noise, i.e., the rock uplift rate is  $U = (h_f -$   
145  $h_i)/50 \text{ Myr}$ . Within the range of possible  $K_f$ , river profiles under uniform uplift either span too  
146 great an elevation range or grade to nearly uniform steepness along their lengths, dissimilar to  
147 the observed fluvial profiles (Figs. 3F and DR7).

148 Considering both the propagating and uniform uplift models using the same erodibility ( $K_f =$   
149  $1.2 \times 10^{-6} \text{ m}^{0.2}/\text{yr}$ ) for comparison, results show that uniform uplift can preserve the relict low-

150 relief surfaces in upstream headwaters (Figs. 3D and DR8A-B), corroborating the findings of  
151 [Whipple et al. \(2017\)](#), but cannot form deep, narrow mainstem valleys with low-relief  
152 interfluvies in their middle and lower reaches ([Sinclair, 2017](#)). This is because, under uniform  
153 uplift, low-relief interfluvies are eventually dissected by a wave of upstream-propagating river  
154 incision (Fig. DR8C). Furthermore, the modeled timing of accelerated exhumation along the  
155 mainstem rivers shows old ages downstream (~35 Ma, V1–V2; Fig. 3E) and younger ages  
156 upstream (~10 Ma, V4), inconsistent with the observed trend of thermochronologic ages ([Li et](#)  
157 [al., 2019](#)).

158 It has alternately been hypothesized that high-elevation, low-relief surfaces may be actively  
159 forming and evolving on the SE Tibetan Plateau due to drainage-area reorganization wrought  
160 by horizontal tectonic shortening ([Yang et al., 2015](#)). While this mechanism may play some  
161 role in promoting the development of low-relief surfaces, our modeling shows that such  
162 surfaces can form even without dramatic drainage area exchange via discrete river capture  
163 events (Fig. 2C). The high-elevation, low-relief surfaces that form in our models do experience  
164 some drainage-area loss and gain via progressive drainage divide migration (Movie DR1).  
165 However, because drainage area exchange occurs gradually at the earlier stage, it does not  
166 significantly modify the remnant low-relief topography, nor does it generate nascent low-relief  
167 surfaces *in-situ*. We further run a model without horizontal tectonic deformation, the high-  
168 elevation, low-relief surfaces can still form, and the modeled  $\chi$ -elevation plot also fits the  
169 observed one (Fig. DR9).

170

## 171 **CONCLUSIONS**

172 Our work brings a new explanation for the genesis of high-elevation, low-relief surfaces, and  
173 shows that these surfaces in the SE Tibetan Plateau are simply a consequence of mountain  
174 growth. Using shortening and uplift parameters (Text DR1) for the specific example of

175 southeastern Tibet, we show that propagating uplift of mountain growth produces broad high-  
176 elevation, low-relief surfaces, spatial and temporal exhumation patterns, and river profile  
177 morphologies matching observations on the SE Tibetan Plateau.

178 Beyond the SE Tibetan Plateau, our modeling may help explain the formation of high-elevation,  
179 low-relief surfaces in the southern Pyrenees (Babault et al., 2005; Bosch et al., 2018), the Andes  
180 (Kennan et al., 1997; Barke and Lamb, 2006), and the Himalayas (van der Beek et al., 2009;  
181 Adams et al., 2016). Progressive, unidirectional uplift in an outward propagating sequence is  
182 likely to occur in these mountain ranges because crustal thickening promotes the formation of  
183 a tectonic ramp at the range margin, with high rock uplift rates that propagate outward and  
184 advance the range front during shortening (e.g., Jammes and Huismans, 2012; Wolf et al., 2021).  
185 Such crustal ramps and outward propagating uplift have been inferred in the southern Pyrenees  
186 (Muñoz, 1992), the Andes (Armijo et al., 2009), and the Himalayan-Tibetan orogen (Wang et  
187 al., 2014; Li et al., 2015). Our modeling shows that this pattern of propagating uplift generates  
188 high-elevation, low-relief surfaces in tectonically active mountain belts, implying potential  
189 preservation of tectonic signals in mountain topography.

190

## 191 **ACKNOWLEDGMENTS**

192 The work is part of the COLORS project funded by TOTAL. We thank Huiping Zhang, who  
193 provides the data of low-relief surfaces. We thank Marin Clark, Benjamin Gérard, and an  
194 anonymous reviewer for their constructive comments.

195 **References**

- 196 Adams, B.A., Whipple, K.X., Hodges, K.V. and Heimsath, A.M., 2016. In situ development of high-elevation, low-relief  
197 landscapes via duplex deformation in the Eastern Himalayan hinterland, Bhutan. *Journal of Geophysical Research: Earth*  
198 *Surface*, 121(2), 294-319.
- 199 Armijo, R., Lacassin, R., Coudurier-Curveur, A. and Carrizo, D., 2015. Coupled tectonic evolution of Andean orogeny and  
200 global climate. *Earth-Science Reviews*, 143, 1-35.
- 201 Babault, J., Van Den Driessche, J., Bonnet, S., Castelltort, S. and Crave, A., 2005. Origin of the highly elevated Pyrenean  
202 peneplain. *Tectonics*, 24(2), doi:10.1029/2004TC001697.
- 203 Barke, R. and Lamb, S., 2006. Late Cenozoic uplift of the Eastern Cordillera, Bolivian Andes. *Earth and Planetary Science*  
204 *Letters*, 249(3-4), 350-367.
- 205 Bosch, G.V., Van Den Driessche, J., Babault, J., Robert, A., Carballo, A., Le Carlier, C., Loget, N., Prognon, C., Wyns, R. and  
206 Baudin, T., 2016. Peneplanation and lithosphere dynamics in the Pyrenees. *Comptes Rendus Géoscience*, 348(3-4), 194-202.
- 207 Clark, M.K. and Royden, L.H., 2000. Topographic ooze: Building the eastern margin of Tibet by lower crustal flow. *Geology*,  
208 28(8), 703-706.
- 209 Clark, M. K., House, M. A., Royden, L. H., Whipple, K. X., Burchfiel, B. C., Zhang, X., Tang, W., 2005. Late Cenozoic uplift  
210 of southeastern Tibet. *Geology*, 33(6), 525-528.
- 211 Clark, M.K., Royden, L.H., Whipple, K.X., Burchfiel, B.C., Zhang, X., Tang, W., 2006. Use of a regional, relict landscape to  
212 measure vertical deformation of the eastern Tibetan Plateau. *Journal of Geophysical Research: Earth Surface*, 111(F03002),  
213 doi:10.1029/2005JF000294.
- 214 Epis, R. and Chapin, C.E., 1975. Surface in the Southern Rocky Mountains. In *Cenozoic History of the Southern Rocky*  
215 *Mountains: Papers Deriving from a Symposium Presented at the Rocky Mountain Section Meeting of the Geological Society*  
216 *of America, Boulder, Colorado (Vol. 144)*. Geological Society of America.
- 217 Fox, M. and Carter, A., 2020. How continuous are the “Relict” landscapes of Southeastern Tibet? *Frontiers in Earth Science*,  
218 8, doi:10.3389/feart.2020.587597.
- 219 Henck, A.C., Huntington, K.W., Stone, J.O., Montgomery, D.R. and Hallet, B., 2011. Spatial controls on erosion in the Three  
220 Rivers Region, southeastern Tibet and southwestern China. *Earth and Planetary Science Letters*, 303(1-2), 71-83.
- 221 Jammes, S. and Huismans, R.S., 2012. Structural styles of mountain building: Controls of lithospheric rheologic stratification  
222 and extensional inheritance. *Journal of Geophysical Research: Solid Earth*, 117(B10), doi:10.1029/2012JB009376.
- 223 Kennan, L., Lamb, S.H. and Hoke, L., 1997. High-altitude palaeosurfaces in the Bolivian Andes: evidence for late Cenozoic  
224 surface uplift. *Geological Society, London, Special Publications*, 120(1), 307-323.
- 225 Li, H.A., Dai, J.G., Xu, S.Y., Liu, B.R., Han, X., Wang, Y.N. and Wang, C.S., 2019. The formation and expansion of the  
226 eastern Proto-Tibetan Plateau: Insights from low-temperature thermochronology. *Journal of Asian Earth Sciences*, 183,  
227 <https://doi.org/10.1016/j.jseaes.2019.103975>

228 Li, Y., Wang, C., Dai, J., Xu, G., Hou, Y. and Li, X., 2015. Propagation of the deformation and growth of the Tibetan–  
229 Himalayan orogen: A review. *Earth-Science Reviews*, 143, 36-61.

230 Liu-Zeng, J., Zhang, J., McPhillips, D., Reiners, P., Wang, W., Pik, R., Zeng, L., Hoke, G., Xie, K., Xiao, P. and Zheng, D.,  
231 2018. Multiple episodes of fast exhumation since Cretaceous in southeast Tibet, revealed by low-temperature  
232 thermochronology. *Earth and Planetary Science Letters*, 490, 62-76.

233 Muñoz, J.A., 1992. Evolution of a continental collision belt: ECORS-Pyrenees crustal balanced cross-section. In *Thrust*  
234 *tectonics* (pp. 235-246). Springer, Dordrecht.

235 Ouimet, W., Whipple, K.X., Royden, L.H., and Granger, D., 2005. Long transient response times of rivers in eastern Tibet to  
236 regional plateau uplift: The effect of mega-landslides, *Geophys. Res. Abstr.*, 7, Abstract 05743.

237 Ouimet, W., Whipple, K., Royden, L., Reiners, P., Hodges, K., Pringle, M., 2010. Regional incision of the eastern margin of  
238 the Tibetan Plateau. *Lithosphere*, 2(1), 50-63.

239 Perron, J.T., Royden, L., 2013. An integral approach to bedrock river profile analysis. *Earth Surface Processes and Landforms*,  
240 38(6), 570-576.

241 Sinclair, H., 2017. Making a mountain out of a plateau. *Nature*, 542(7639), 41-42.

242 Schoenbohm, L.M., Burchfiel, B.C. and Liangzhong, C., 2006. Propagation of surface uplift, lower crustal flow, and Cenozoic  
243 tectonics of the southeast margin of the Tibetan Plateau. *Geology*, 34(10), 813-816.

244 Tian, Y., Kohn, B.P., Gleadow, A.J. and Hu, S., 2014. A thermochronological perspective on the morphotectonic evolution of  
245 the southeastern Tibetan Plateau. *Journal of Geophysical Research: Solid Earth*, 119(1), 676-698.

246 van Der Beek, P., Van Melle, J., Guillot, S., Pêcher, A., Reiners, P.W., Nicolescu, S. and Latif, M., 2009. Eocene Tibetan  
247 plateau remnants preserved in the northwest Himalaya. *Nature Geoscience*, 2(5), 364-368.

248 Wang, C., Dai, J., Zhao, X., Li, Y., Graham, S.A., He, D., Ran, B. and Meng, J., 2014. Outward-growth of the Tibetan Plateau  
249 during the Cenozoic: A review. *Tectonophysics*, 621, 1-43.

250 Whipple, K.X., 2001. Fluvial landscape response time: how plausible is steady-state denudation? *American Journal of Science*,  
251 301(4-5), 313-325.

252 Whipple, K.X., DiBiase, R.A., Ouimet, W.B. and Forte, A.M., 2017. Preservation or piracy: Diagnosing low-relief, high-  
253 elevation surface formation mechanisms. *Geology*, 45(1), 91-94.

254 Wobus, C., Whipple, K.X., Kirby, E., Snyder, N., Johnson, J., Spyropolou, K., Crosby, B., Sheehan, D. and Willett, S.D., 2006.  
255 *Tectonics from topography: Procedures, promise, and pitfalls. Special Papers-Geological Society of America*, 398, 55-74.

256 Wolf, S. G., Huismans, R. S., Muñoz, J.-A., Curry, M. E., and van der Beek, P. (2021). Growth of collisional orogens from  
257 small and cold to large and hot— inferences from geodynamic models. *Journal of Geophysical Research: Solid Earth*, 126,  
258 e2020JB021168

259 Yang, R., Willett, S.D. and Goren, L., 2015. In situ low-relief landscape formation as a result of river network disruption.  
260 *Nature*, 520(7548), 526-529.

261 Yuan, X.P., Braun, J., Guerit, L., Rouby, D., Cordonnier, G., 2019. A new efficient method to solve the stream power law  
262 model taking into account sediment deposition. *Journal of Geophysical Research: Earth Surface*, 124, 1346-1365.

263 **Figure 1. The study area in the Tibetan Plateau.** **A**, Map of the Tibetan Plateau. **B**, Closer view of  
264 the study area with the high-elevation, low-relief surfaces on the SE Tibetan Plateau. Black curves show  
265 the catchment boundaries of the Salween, Mekong and Yangtze Rivers. Trunk channels of the Three  
266 Rivers are colored with the channel steepness  $k_{sn}$  from Equation 1 (see text for details). Yellow shading  
267 shows low-relief surfaces as identified in [Clark et al. \(2006\)](#). **C**,  $\chi$ -elevation plot (Equation DR7) using  
268  $m/n = 0.4$  (yellow: Salween; green: Mekong; magenta: Yangtze) (see text for details). The same data for  
269 a range of values of  $m/n$  are shown in Fig. DR2. **D-F**, Mainstem river profiles, the maximum and mean  
270 topography of 20-km wide swaths parallel to rivers with mean annual precipitation.

271 **Figure 2. Landscape evolution model of the SE Tibetan Plateau in response to southeastward**  
272 **propagating uplift and horizontal shortening using FastScape (Yuan et al., 2019).** **A,** River network  
273 and elevation shown at 50 Ma, 25 Ma, and 0 Ma (Movie DR1). A cross section of rock uplift rate  $U$   
274 (mm/yr) is plotted below the panels. **B,** Channel steepness  $k_{sn}$  ( $m^{0.8}$ ) in Equation 1 (Movie DR2). **C,**  $\chi$   
275 values using Equation DR7 and the low-relief surfaces (yellow shading areas) with surface slope  $<4^\circ$   
276 (Movie DR3). The modeled low-relief surfaces exist in the headwaters and interfluves above deep valley,  
277 consistent with observations (Fig. 1B). Box area shows the modeled  $\chi$ -elevation plots of interior and  
278 exterior rivers in Fig. DR6A. **D,** The river profile at 0 Ma and maximum elevation in a 150-km wide  
279 swath profile, as well as erosion rate (blue) along the river profile. Black and colored dots show several  
280 representative locations of landscape in **A**. **E,** Topography at 30 Ma, 15 Ma, and 0 Ma located at the  
281 dashed lines in **A**.

282 **Figure 3. Spatial and temporal exhumation patterns and  $\chi$ -elevation comparisons for two modeled**  
283 **uplift scenarios.** **A**, Total exhumation over 50 Myr of modeled landscape evolution using the  
284 propagating uplift scenario, with black and colored dots showing the locations of exhumation histories  
285 displayed in **B**. The cyan and orange dots are situated on low-relief interfluvies between deep valleys  
286 and headwaters, respectively. **C**, Comparison of modeled and observed  $\chi$ -elevation plots for the  
287 mainstem rivers using the erodibility  $K_f = 1.2 \times 10^{-6} \text{ m}^{0.2}/\text{yr}$ . **D**, Total exhumation over 50 Myr of the  
288 uniform uplift scenario using the same erodibility, with black dots showing the locations of exhumation  
289 histories along the mainstem rivers in **E**. **F**, Comparison of modeled and observed  $\chi$ -elevation plots for  
290 the mainstem rivers.

# Figure 1

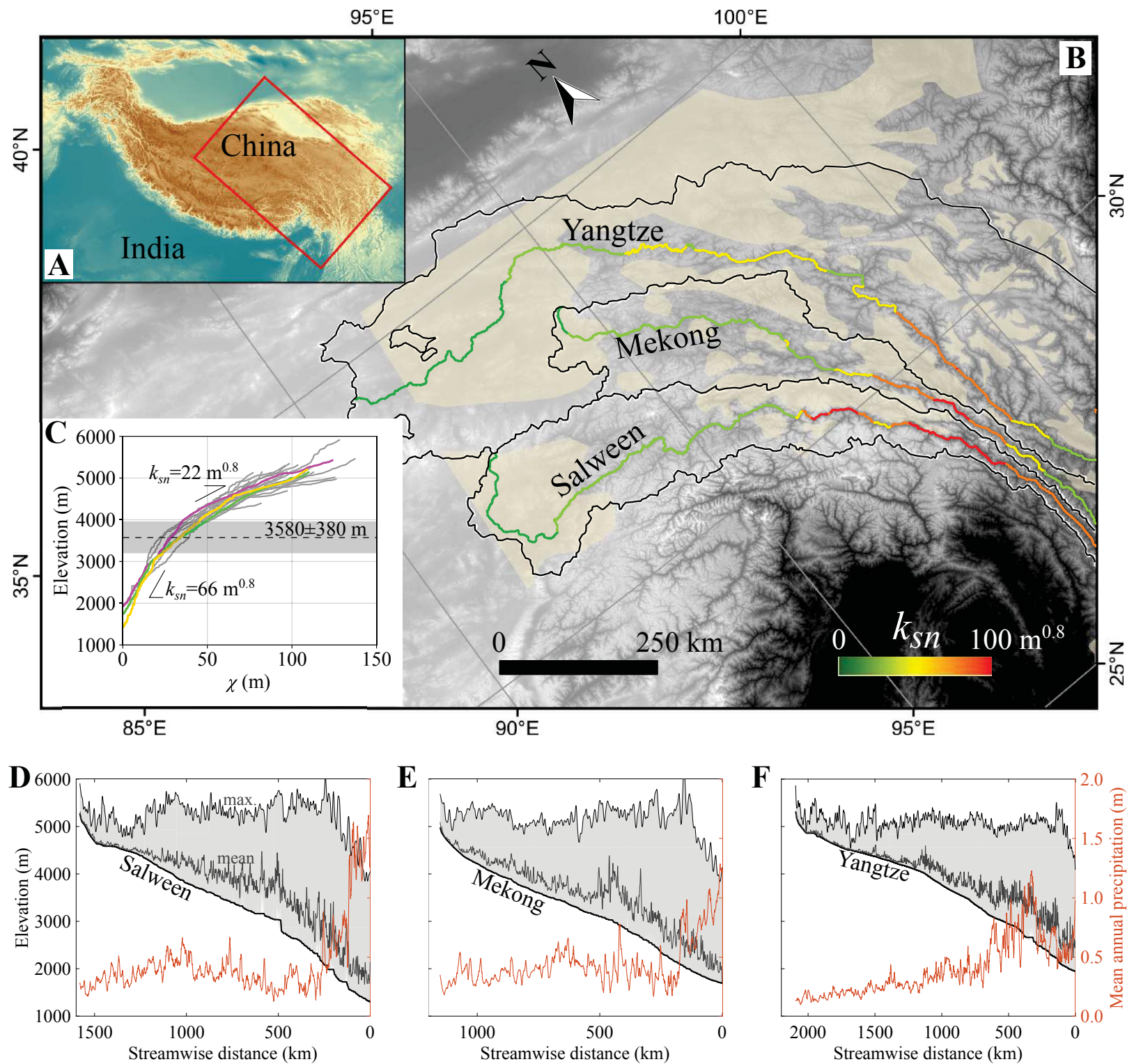


# Figure 2

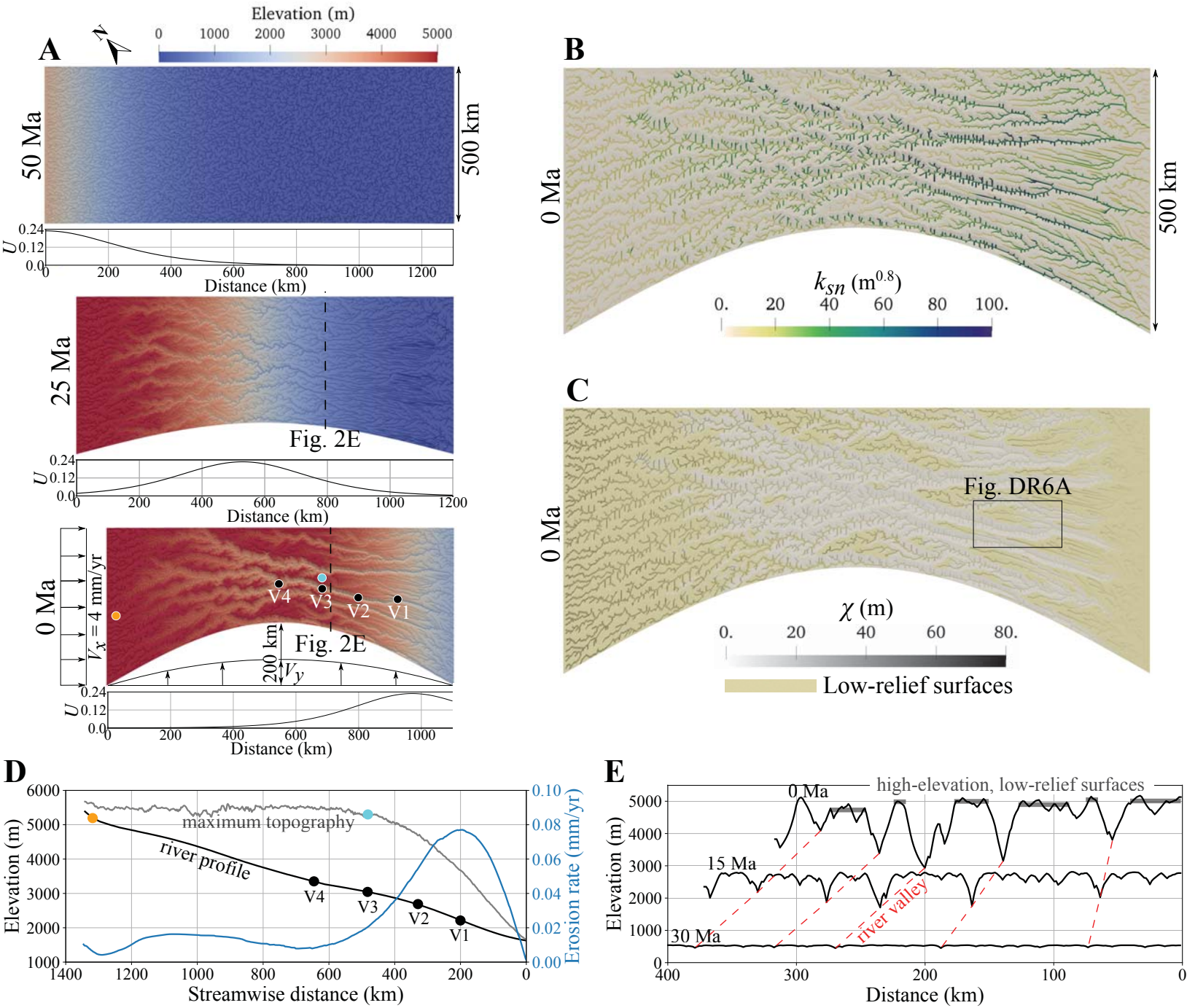


# Figure 3

